EUROPEAN ORGANISATION FOR NUCLEAR RESEARCH

CERN-ISR-VA/74-40
Closed distribution

THE GAS CURTAIN GENERATOR OF THE BEAM PROFILE MONITOR IN THE ISR*

by

B. Vosicki and K. Zankel

Abstract

A supersonic beam source is described which generates continuously a gas curtain 0.7 mm thick and 64 mm wide. The maximum intensity is 10^{20} atoms/ster.s. A commonly used theoretical model for the determination of the transition surface cannot predict the results obtained. An indirect determination of the collision cross section for sodium - sodium scattering yields a value of 28×10^{-16} cm^2, which is forty times lower than that measured by Buck and Pauly[7]. Some results about the condensation behaviour of sodium vapour on metallic substrate surfaces are reported.

Geneva, 17th July 1974

---

* to be submitted for publication in the 'Review of Scientific Instruments'.

Table of Contents

1. INTRODUCTION

Observation of the stored proton beam in the ISR required the construction of a molecular beam curtain as a target. The curtain should be generated by an atomic beam source yielding an intensity of 1.2 atoms/ster.s, which is about a factor of 100 higher than that from the best existing continuous sources. We hoped to reach the design figure in using a supersonic slit source in conjunction with a powerful condensation pumping system.

2. EXPERIMENTAL REQUIREMENTS

Dimensions of the beam :

A molecular beam 6.4 cm wide, 0.7 mm thick having a divergence of 0.7 mrad and an inclination of 45° to the horizontal plane is needed in an ultrahigh vacuum system (10^{-11} torr).

Intensity of the beam :

The 0.7 mrad divergence required dictates that the source be 1 m away from the point where the density of 10^{12} atoms/cm^3 is wanted. It follows that such a source must yield an intensity of $1.2\ 10^{21}$ mol/ster.s assuming a maximum velocity of 1200 m/s corresponding to a supersonic outflow of sodium vapour at $550^{\circ}C$.

Comments :

Such high intensities can only be achieved by means of a supersonic flow, where some of the random thermal motion of the gas atoms is converted into an ordered motion. This process takes place when there are enough collisions between the atoms of the gas during the outflow from a pressurized vessel. However, the effect of the ordered motion is lost when the produced "jet" encounters too many particles on its passage from the source to the point of utilisation. Therefore a very powerful pumping system is needed, if one wants to produce a dense molecular beam of large dimensions. In fact the only way to pump high gas flow rates is to condense the gas. Consequently sodium vapour was chosen as an "easily" condensable gas, which satisfies another imposed boundary condition, namely that the vapour pressure of the condensed gas at room temperature is lower than 10^{-9} torr.

3. THEORETICAL CONSIDERATIONS

The problem of supersonic flow of gas into vacuum is described by the Boltzmann equation, but no mathematical solution has been found so far. W. Brook and R. Oman[1] solved an approximate Boltzmann equation but their results are not conclusive. The only existing simple model, developed by R. Oman and V. Calia[2] has satisfactorily predicted the velocity distribution emanating from an axisymmetric supersonic flow, confirmed experimentally by J. Anderson and J. Fenn[3]. In the following we consider the Oman-Calia model in order to get some qualitative feeling about the relationship between the intensity at a point far downstream of the flow and the source pressure. The supersonic outflow into vacuum is characterised by two regions :

1. A hydrodynamic flow region : there the collisions between molecules are predominant and the conversion of the random thermal motion into an ordered one takes place. The variance of the velocity distribution function decreases with the number of collisions, and the angular distribution function $F(\varphi)$ centres around the mean flow velocity vector w (see Fig. 1). The Mach number, which is the ratio of the flow velocity to the speed of sound, is an appropriate measure for this conversion process.
2. A molecular flow region : there the collisions between molecules can be neglected.

3.1 Transition surface :

The surface which delimits the two regions is called transition surface. Oman and Calia picture it in the following manner: the increase in uniformity of molecular velocities is limited by the collision frequency regardless of the predictions of Mach number gradient from hydro-dynamic flow theory. In particular, they state that the decrease in velocity of one molecule with respect to the mean flow velocity is proportional to this relative velocity $\bar{c}$ multiplied by an effectiveness parameter ε.

$$d\bar{c} = - \varepsilon \bar{c} \frac{dn}{N}$$

dn denotes the number of collisions and N the number of particles per volume.

Because not all collisions contribute to decrease $\bar{c}$, ε must be smaller than one. Comparing their experimental results, Anderson and Fenn[3] found ε to be 0.25. Relating $\bar{c}$ to the local Mach number M the above equation transforms (for high Mach numbers) to

$$\left(\frac{dM}{dx}\right)_{max} \leq \sqrt{\frac{8}{\pi\gamma}} \frac{\varepsilon}{\lambda_x} \qquad (1)$$

where γ is the adiabatic constant equal to 5/3 for a monoatomic gas, λ_x is the mean free path at the distance x from the source.

They suppose that a transition surface exists at the point where the Mach number gradient from continuum predictions is equal to the one from equation (1).

The approximate continuum equations for the case of a point source and a line source are as follows :

- point source : the flow from a circular nozzle of diameter D can be assimilated to a flow originating from a point source Q (see Fig. 1). The Mach number M, if sufficiently large, varies with distance x approximately as

$$M = 3.2 \left(\frac{x}{D}\right)^{2/3} \qquad (2)$$

Equation (1) and the derivative of equation (2) combined with the equation for isentropic flow expansion enable to calculate the distance x_1 to the transition surface Γ. The result is

$$\frac{x_1}{D} = 0.238 \left(\frac{\varepsilon}{Kn_o}\right)^{0.6} \qquad (3)$$

The corresponding Mach number is given by

$$M_1 = 1.23 \left(\frac{\varepsilon}{Kn_o}\right)^{0.4} \qquad (4)$$

Kn_o is the Kundsen number, which is the ratio of the viscosity mean free path to the source diameter D calculated for the stagnation temperature in the source.

- line source of infinite length : in an analog fashion to the point source the outflow from a slit can be assimilated to a flow originating from a line source. The above arguments are now applied to determine the transition surface for the case of a line source of infinite length. The potential equation for cylindrical coordinates can be solved assuming angular independence. Its solution is :

$$\frac{x}{h} = \frac{(M^2+3)^2}{2^5 M}$$

where h is the width of the slit. For large M the above equation simplifies to

$$M = 2^{5/3} \left(\frac{x}{h}\right)^{1/3} \qquad (5)$$

From relation (1) and the derivative of equation (5) the distance x_1 and M_1 are given by

$$\frac{x_1}{h} = 0.0072 \ (\varepsilon/Kn_o)^3 \qquad (6)$$

$$M_1 = 0.023 \ (\varepsilon/Kn_o) \qquad (7)$$

3.2 Theoretical density and flux at a point P downstream

If in the molecular flow region there are no interactions with the residual gas or within the beam itself, the density n_p and the flux J_p at a point P, which sees the surface Γ under the solid angle Ω (Fig. 1) are given by :

$$J_p = n_\tau \bar{v}_o \frac{\Omega}{4\pi} g(M_1) \qquad (8)$$

where $\bar{v}_o$ is the mean velocity of the molecules at stagnation conditions and n_τ is the density at the surface Γ.

$$n_p = n_\tau \frac{\Omega}{4\pi} G(M_1) \tag{9}$$

$$g(M_1) = \frac{1}{\sqrt{1 + \frac{\gamma+1}{2} M_1^2}} \left\{ e^{-u^2} (1 + u^2) + \sqrt{\pi}\, u(1 + \text{erf } u)(\tfrac{3}{2} + u^2) \right\} \tag{10}$$

where $u^2 = \frac{1}{2}\gamma M_1^2$

$$G(M_1) = \frac{2}{\sqrt{\pi}} u\, e^{-u^2} + (1 + 2u^2)\,(1 + \text{erf } u) \tag{11}$$

M_1 is the flow Mach number at the transition surface. The functions g(M) and G(M) derived for the assumption that the angle θ is small (see Fig. 1), express the collimation effect due to the superposition of a flow velocity w upon the Maxwellian velocity distribution in the gas. They become proportional to M^2, if M is sufficiently great ($M > 4$). From relation (9) the following proportionality is derived :

$$n_p \simeq n_\tau M_1^2 \tag{12}$$

n_τ is related to the density in the source by the isentropic continuum equation.

3.3 Comparison of a circular and a slit source

For a monoatomic gas we get

$$n_\tau \simeq n_o M_1^{-2} \tag{13}$$

Combining equation (12) and (13) yields

$$n_p \simeq n_o M_1^{-1} \tag{14}$$

and since $$Kn_o^{-1} \simeq n_o$$

we obtain for the axisymmetric case from equation (4) the relation :

$$n_p \simeq n_o^{0.6} \tag{15}$$

whereas for the planesymmetric flow from equation (7) it follows that the density n_p does not depend on the source density n_o. The latter result is surprising. One can argue that there exists no slit source of infinite length; in fact, if the transition distance x_1 becomes much greater than the slit length, one approaches the case of a point source. However, neither our experimental results for a slit source nor those from H.J. Lasalle[4] and other workers for a circular nozzle agree qualitatively with the result from the model. The shortcomings of the theory lies probably in the fact that the effectiveness ε, which depends on the shape of the velocity distribution function, varies strongly during the expansion process.

3.4 Scattering

The molecules of the beam are scattered by the molecules from the beam itself as well as by the molecules from the background.

3.4.1 Beam - background scattering

The number of collisions per second of the beam molecules with the residual gas over a distance dx is given by

$$n\bar{c}\,\frac{dx}{\lambda_R}$$

where

$$\frac{1}{\lambda_R} = Q(v_m)\; H\left(6, \frac{v_m}{v_{mR}}\right) \cdot n_R$$

n_R is the density of the residual gas, $\bar{c}$ is the mean speed of the molecules in the beam, Q is the total cross section as derived for an interaction potential of the type (12, 6). It depends on the speed

$$v_m = \sqrt{\frac{2RT}{M}} \qquad (16)$$

according to the power law of $-2/5$, M is the molecular mass and T_o is the temperature in the source. The function H is tabulated in Massey, p. 1348[5]. v_{mR} is given by the same expression as (16) with reference to the residual gas.

3.4.2 Intra-beam scattering

The number of collisions per second among molecules in the beam over a distance dx is given by

$$n^2 \bar{c}\, f(M)\, Q\, v^{2/5}\, dx$$

where v is the speed given by (16), at which the total cross section Q has been determined. f(M) is a function of the Mach number and can be calculated from the expression in reference 6 if the relative velocity dependence of the cross section is taken into account.

3.4.3 Effect of collisions on density

We consider that each particle suffering a collision leaves the beam. Then the total decrease dn in density over a distance dx is given by :

$$dn = -\left(f(M) v^{2/5} Q\, n^2 - \frac{n}{\lambda_R}\right) dx - n\,\frac{d\Omega}{\Omega} \qquad (17)$$

where $\Omega = \text{arc tg}\ \dfrac{h \cdot \ell}{2x\sqrt{h^2 + \ell^2 + 4x^2}}$

Ω is the solid angle under which is viewed a slit of dimensions $h \times \ell$ from a distance x. The solution of the Benouilli equation (17) with the initial condition

$$x = 0 \qquad n = n_o/2$$

is given by

$$n = n_o\, \frac{\Omega(x)\, \exp\left(-\dfrac{x}{\lambda_R}\right)}{1 + f(M)\, v^{2/5}\, Q n_o \displaystyle\int_o^x \Omega(t)\, \exp\left(-\frac{t}{\lambda_R}\right) dt} \qquad (18)$$

t is the integration variable.

In the case of sodium - sodium scattering the total cross section is 1100.10^{-16} cm^2 at a reference speed of $3.87\ 10^4$ cm/s [7]. If we assume that the partial pressure of sodium constitutes the major part of the residual gas in our system, then it must be less than several 10^{-6} torr in order that beam scattering over a distance of 35 cm stays negligible.

The contribution of self-scattering will be discussed in conjunction with the interpretation of the measurements. Here we give an approximation of the integral in the denominator of expression (17). Assuming that the scattering by the residual gas can be neglected this integral is approximated by

$$\int_0^{\ell/2} \mathrm{tg}^{-1}\left(\frac{h}{2t}\right) dt = \frac{\ell}{2}\ \mathrm{ctg}^{-1}\left(\frac{\ell}{h}\right) + \frac{h}{4}\ \ell n\left[1 + \left(\frac{\ell}{h}\right)^2\right]$$

because $\Omega(t)$ decreases rapidly with t.

4. DESCRIPTION OF APPARATUS

The apparatus was constructed to have the following characteristic numbers : Knudsen number of the source vapour 0.01, slit length 6.4 cm. This implies a gas flow of one g/s to be generated by a heating power of 4.2 kW. Therefore the heating and condensation facilities were designed for a power of 5 kW. The principal parts of the source are shown in Fig. (2).

4.1 Boiler

Sodium vapour is generated in the boiler (2) and superheated in a chamber (3). This part of the boiler is made out of Numonic 75. On its outer surface there are grooves in which the coaxial heating elements (2 mm in diameter) plus spare ones are imbedded. These thermocoaxial cables are pressed down in their grooves by small stainless steel bars and are covered with a 2 mm thick nickel layer deposited by means of plasma spraying.

4.2 Beam shaping elements

The exit nozzle (12) which has a slit width of 0.7 mm, a length of 64 mm and a lip length of 0.2 mm is screwed to the super-heater chamber. A copper foil is interposed to make a seal and to assure a good thermal contact. The beam scraper (6) is housed in the cover (7). Its slit, which has the same dimension as that of the nozzle is heated by a thermocoaxial cable to a temperature where clogging by sodium is excluded. The second collimation slit is not represented in the figure. A shutter (8) which can be actuated via a stainless steel bellows can block the passage of the sodium beam.

4.3 Condensation and pumping system

If the residual partial pressure of sodium is to stay below 10^{-5} torr, sodium vapour must be pumped by the condensation surfaces with a sticking factor approaching unity. The first experiments, where large copper condensation surfaces were installed have revealed that the partial pressure of sodium was too high and that beam - background scattering occurred. Therefore investigations on the condensation behaviour have been undertaken in order to determine the influence of the substrate surface and its temperature as well as the influence of the flux ratio of sodium vapour to the residual gas arriving on the surface.

The surfaces examined were : gold, silver, indium and tin deposited on copper plates, one copper plate cleaned in chromic sulfuric acid and another copper plate cleaned in a solution of oxalic acid and perhydrol. Before exposure to sodium vapour, the samples were baked at $300^{\circ}C$. When sodium vapour has been admitted via a diaphragm, the mode of condensation was visually observed through a heated saphire window. The results are given in the table below.

Substrate Surface	Au	Ag	In	Su	Cu
Decomposition temperature of oxides	200°C Au_2O 150°C Au_2O_3	300°C Ag_2O	850°C In_2O_3	700°C SuO 1127°C SuO_2	1026°C CuO 1235°C Cu_2O
mode of condensation	film	film	droplet	droplet	droplet

We see the reason for film condensation in the fact that the oxides of gold and silver are already decomposed at the bakeout temperature and that the sodium vapour arrives on the metallic surface where it is bound by the noble metal. Furthermore, the sticking coefficient α was determined as a function of the ratio R of the flux of sodium to the flux of residual gas molecules. The composition of the latter has been analysed and the following mass spectrum has been found at a nitrogen equivalent pressure of 5×10^{-8} torr.

mass number	2	14	15	16	17	18	28	40	44
percentage referred to molecular density	89.3	0.4	0.6	1	0.7	1.9	6.4	0.3	0.2

The predominant residual gas was molecular hydrogen. One sees from Fig. (3), where the results of these measurements have been plotted, that the sticking coefficient decreases with a decreasing flux ratio. We see the reason for this behaviour that at a low flux ratio R the substrate surface is covered by physically adsorbed hydrogen, which impedes the full accommodation of the arriving sodium atoms. The measurements did not show any dependence on the substrate temperature. We conclude, therefore, that sodium condenses on clean metallic surfaces and on clean sodium covered surfaces with a sticking probability of one.

As a consequence of the above measurements the condensation surfaces were kept small and the partial pressure of the non-condensable gases had to be kept low. Therefore a good pumping system has been installed consisting of an ion pump with a pumping speed of 400 ℓ/s and a turbomolecular roughing pump. The residual gas pressure was thus maintained below 10^{-9} torr. This has been measured by an ionisation gauge and the residual gas composition was checked by a mass spectrometer. The partial sodium vapour pressure in the vessel was measured by two gauges, which were permanently heated to 200°C in order to impede sodium vapour condensation in them. As one sees from Fig. (2), most of the sodium vapour is condensed on a thick copper disc (4), cooled by an oil circuit. In the middle of this disc is an opening which is just so big that the biggest sodium droplets cannot clog it. The rest of the vapour condenses on the cooled plates (10) surrounding the beam. Since the power dissipation per unit of surface is high, the cooling circuit, consisting of a single copper tube (9) was embedded in the copper plates and silver brazed under vacuum. In order to prevent the dissolution of the silver solder by the sodium, all silver brazed parts were nickel plated.

4.4 Control and sodium transfer system

4.4.1 Temperature control

The condensation plates are maintained above the melting temperature of sodium of 96°C. This is done in regulating on the one hand the flow rate of the oil circuit and on the other the power in the coaxial heating elements, which are also embedded on the condensation plates. All heaters are regulated continuously by triac controllers. The sodium temperature in the boiler is measured by a thermocouple fixed at the bottom of the tube (14).

4.4.2 Sodium level

The tube (14) guides also a float (1) with a permanent ring magnet inside. A hollow cylinder in soft iron suspended in the tube can follow the movements of the float indicating the sodium level

in the boiler. In the condensation vessel the level of sodium is measured by a nickel plated copper bar (13), where a thermocouple has been fixed near the middle. When the point of the bar dips into the liquid sodium, a temperature change is recorded which in turn is linked to the sodium level in the condensation chamber.

4.4.3 Sodium transfer and filling system

It is shown schematically in figure 4. The sodium which is condensed in the vessel (2) is pumped back to the boiler (3) by a small electromagnetic pump (4) yielding a pressure of several hundred torr and a flow rate of several grams per second. One of the main impurities of the sodium circuit is sodium oxide. The solubility of sodium oxide in sodium is decreasing with decreasing temperature so that danger exists in that it precipitates in cooler places where it can clog the tubing (e.g. the sodium pump). Therefore sodium is continuously cleaned by a filter of sintered stainless steel (5) having a pore diameter of 5 microns. The filter is maintained at the temperature of 130°C, which favours the precipitation of sodium oxide. Sodium is filled into the boiler in forcing it up from the reservoir (10) by means of 100 torr pressure of pure argon. The sodium level in the reservoir is determined by the electric resistance measurement of a stainless steel wire plunged into the sodium.

5. RESULTS

5.1 Beam detection

A Langmuir-Taylor surface ionisation detector was used to measure the intensity of the sodium beam. Its filament was a platinum ribbon 0.8 mm wide and 0.05 mm thick which intercepted the beam at an angle of 90°.

5.2 Scaling

The results of the measurements are recorded in figure 5, where the intensity of the beam at a distance of 90 cm from the source is plotted against the "stagnation conditions". The values on the ordinate have been scaled in the molecular flow region, where the intensity $p/\sqrt{T_o}$ is related to the source pressure p_o (torr) and the temperature T_o (^oK) by the following expression

$$\frac{p}{\sqrt{T_o}} = \left(\frac{\Omega}{4\pi}\right) \cdot \frac{p_o}{\sqrt{T_o}}$$

5.3 Discussion

5.3.1 Molecular flow :

From figure (5) it can be seen that the experimental curve deviates from the above linear flow already at the pressure corresponding to the source Knudsen number of 10. The latter has been computed from the gas kinetic cross section of sodium of $23.5\ 10^{-16}$ cm^2. Since the jet intensity measured at a Knudsen number of 1 differs by a factor of three from the theoretical value, the measurements have been repeated several times. The temperature of the liquid sodium in the boiler was measured with an error smaller than $\pm\ 5^o$ corresponding to an error in pressure of $\pm$ 20%. Background scattering had to be excluded, because the pressure measured at two points on the vessel was smaller than 10^{-6} torr and the results did not change when the condensation surfaces were cooled with liquid nitrogen. Therefore intra-beam scattering must be responsible for the observed deviation. The dashed curve in figure (5), which is the attenuated beam intensity calculated for a total collision cross section of $28\ 10^{-16}$ cm^2, fits fairly well the experimental observation. Furthermore, such an explanation is conformed by observation of the sodium beam after the first collimation slit. When the sodium beam is condensed on a glass plate, a halo around the slit image begins to appear at a source Knudsen number of 5, suggesting that intra-beam scattering has taken place.
However, the supposed cross section

of 28 10^{-16} cm^2 is some 40 times smaller than the one measured by Buck and Pauly[7]! This discrepancy cannot be explained by the argument that the measured flux was also composed of scattered particles. In fact the detector has an angular resolution of 1.2 steradians perpendicular to the plane of the beam and is seen by a scattered particle under a solid angle of only 10^{-6} steradians. Since the attenuation from self-scattering is less than 5.10^{-3} the chance of collecting scattered particles is negligibly small.

5.3.2 Supersonic flow

When the source Kundson number begins to be smaller than 0.2, an increase in intensity following a power law of 0.9 is observed which is as we have already mentioned, in contradiction to the theoretical forecast from the model of Oman and Calia.

6. CONCLUSIONS

The intensity of the continuously working supersonic beam source is about 10^{20} atoms/ster.s which is a better performance than that of any other source described. However, it is still a factor of ten lower than what was originally aimed at. Intensity measurements as a function of the source pressure in the molecular flow region at a Knudsen number of five revealed intra-beam scattering. The determined collision cross section differs very much from the one measured by Buck and Pauly[7]. The intensity behaviour in the supersonic flow region is in contradiction with the simple theoretical model put forward by Oman and Calia. The source could be operated satisfactorily only after studies of the condensation of sodium revealed that the sticking factor is independent of the substrate temperature and approaches unity when the flux of the metal vapour is much bigger than that of the residual gas, and the condensation surface is of a special quality.

Note

Two such sources have been built and are operating almost continuously as a part of the beam profile observation equipment in the ISR at CERN. The sodium beam passing across the vacuum chamber of the ISR does not perturb its ultrahigh vacuum condition, which was one of the design requirements.

7. ACKNOWLEDGEMENTS

We thank R. Huguénin and J-M. Robert for valuable assistance in setting up the apparatus. The help of M. Genet in designing the apparatus is also greatly appreciated. Finally, the authors would like to thank E. Fischer for his many discussions and encouragements.

8. REFERENCES

1) J.W. Brook and R. Oman, Rarified Gas Dynamics, edited by J.H. de Leeuw (Academic Press, New York 1965), pp. 125 - 139.

2) R. Oman, V.S. Calia, Grumman Research Department Report, RE-166 (1963).

3) J.B. Anderson and J.B. Fenn, Phys. Fluids 8 (May 1965), 780-87.

4) H.J. Lassalle, Dissertation, Techn. Universität, Braunschweig (1969), p. 74.

5) H.S. Massey et al, Electronic and ionic impact phenomena, 2nd edition, Vol. III, Oxford 1971.

6) K. Zankel, J. Phys. B., Vol. 5, Jan. 1972, p. 74.

7) V. Buck and H. Pauly, Z.F. Physik, 185 (1965) 155 - 168.

FIGURE CAPTIONS

Figure 1 Scheme of the model for the supersonic outflow from an idealised line source Q with velocity w, h slit width, F transition surface, P observation point at solid angle Ω, dn_τ density at transition surface.

Figure 2 Schematic view of beam source :

1 float; 2 boiler; 3 superheater; 4 circular condensation surface; 5 flange for vacuum pipe; 6 first collimating slit; 7 cover; 8 beam stopper; 9 cooling tube; 10 condensation box; 11 exit nozzle; 12 sodium level indicator; 13 tube for magnetic indication of sodium level in boiler and temperature measurement of the liquid sodium.

Figure 3 Sticking coefficient α as a function of the ratio R of the flux of residual gas molecules.

Figure 4 Scheme of sodium source, sodium transfer line and vacuum system:

1 ionisation gauge; 2 superheater; 3 boiler; 4 electromagentic pump; 5 filter; 6 flexible tube; 7 bellows valve of stainless steel; 8 electric feedthrough; 9 measuring wire; 10 sodium reservoir; 11 mass spectrometer; 12 400 ℓ/s ion pump; 13 beam stopper; 14 argon bottle; 15 molecular pump; 16 turbomolecular pump.

Figure 5 Intensity $\frac{p}{\sqrt{T_o}}$ at a distance of 900 mm from the source as a function of source pressure p_o and temperature T_o; dashed curve represents the calculated beam intensity fitted for a total collision cross section of 28×10^{-16} cm^2.

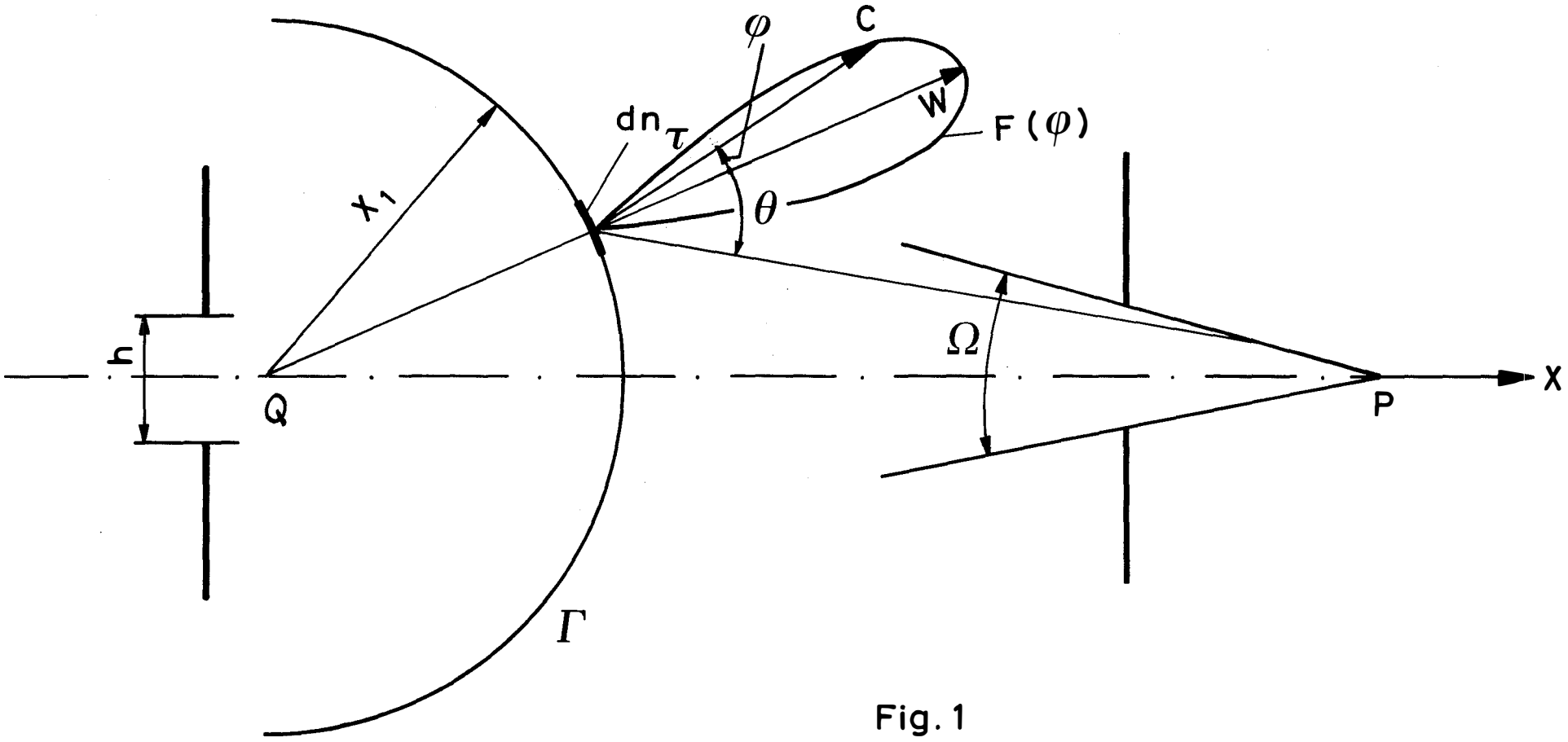

Fig. 1

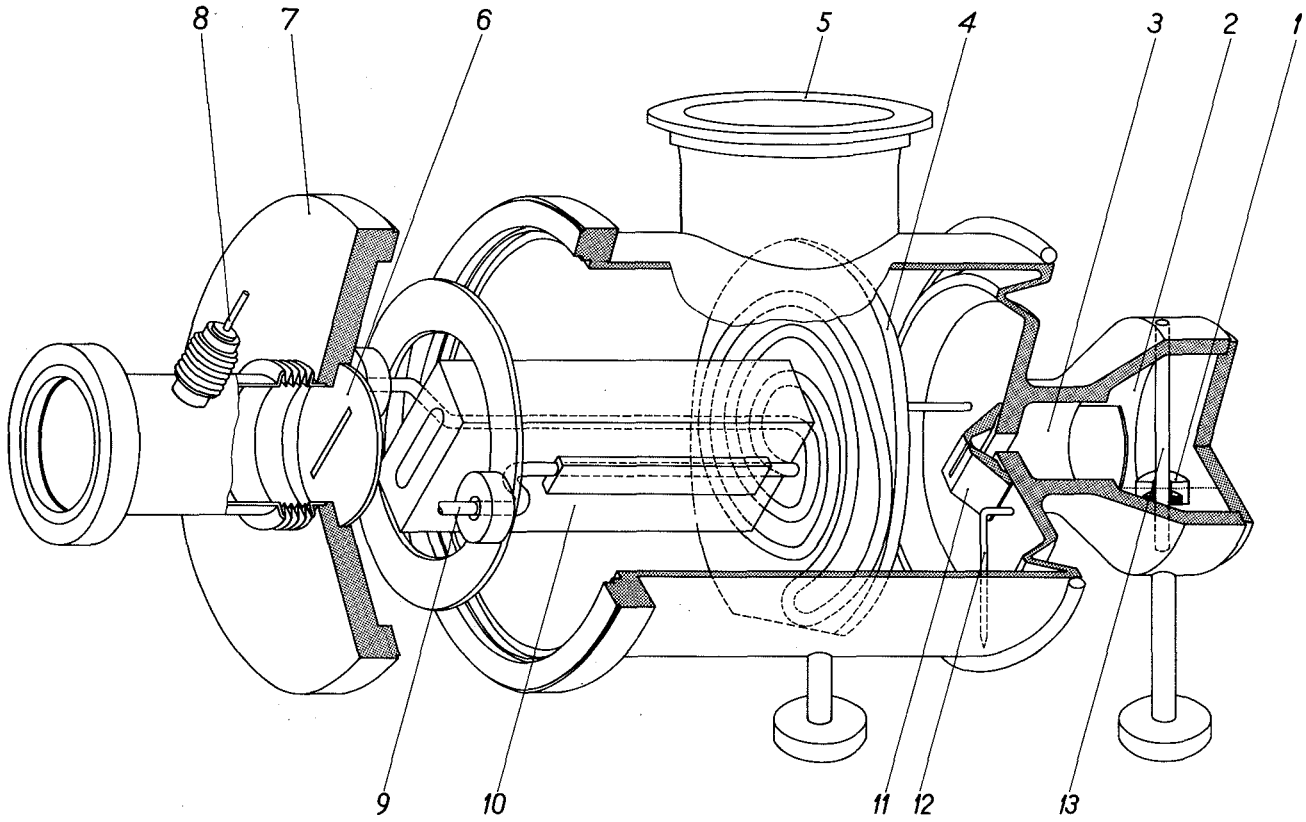

Fig. 2

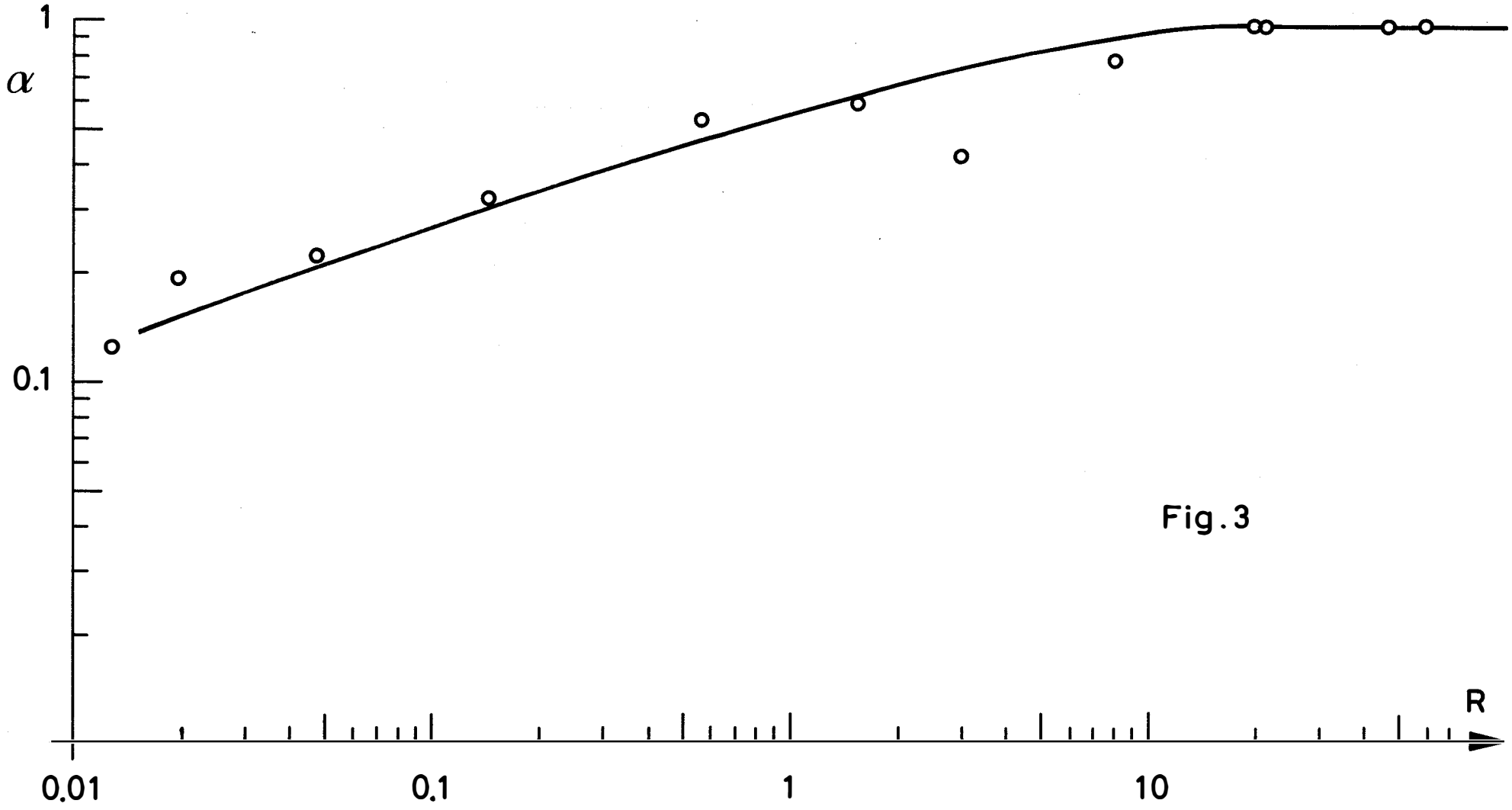

Fig. 3

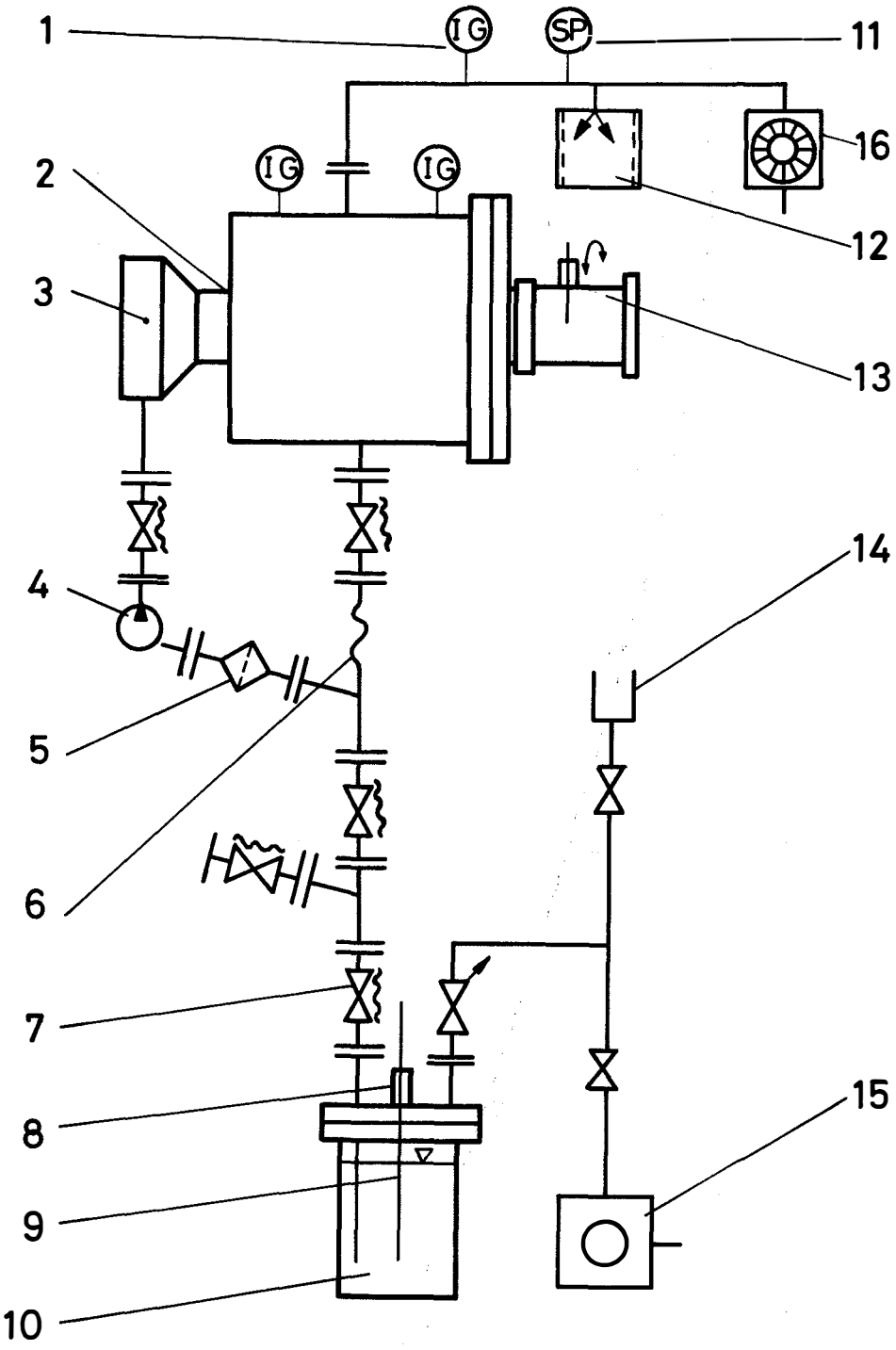

Fig. 4

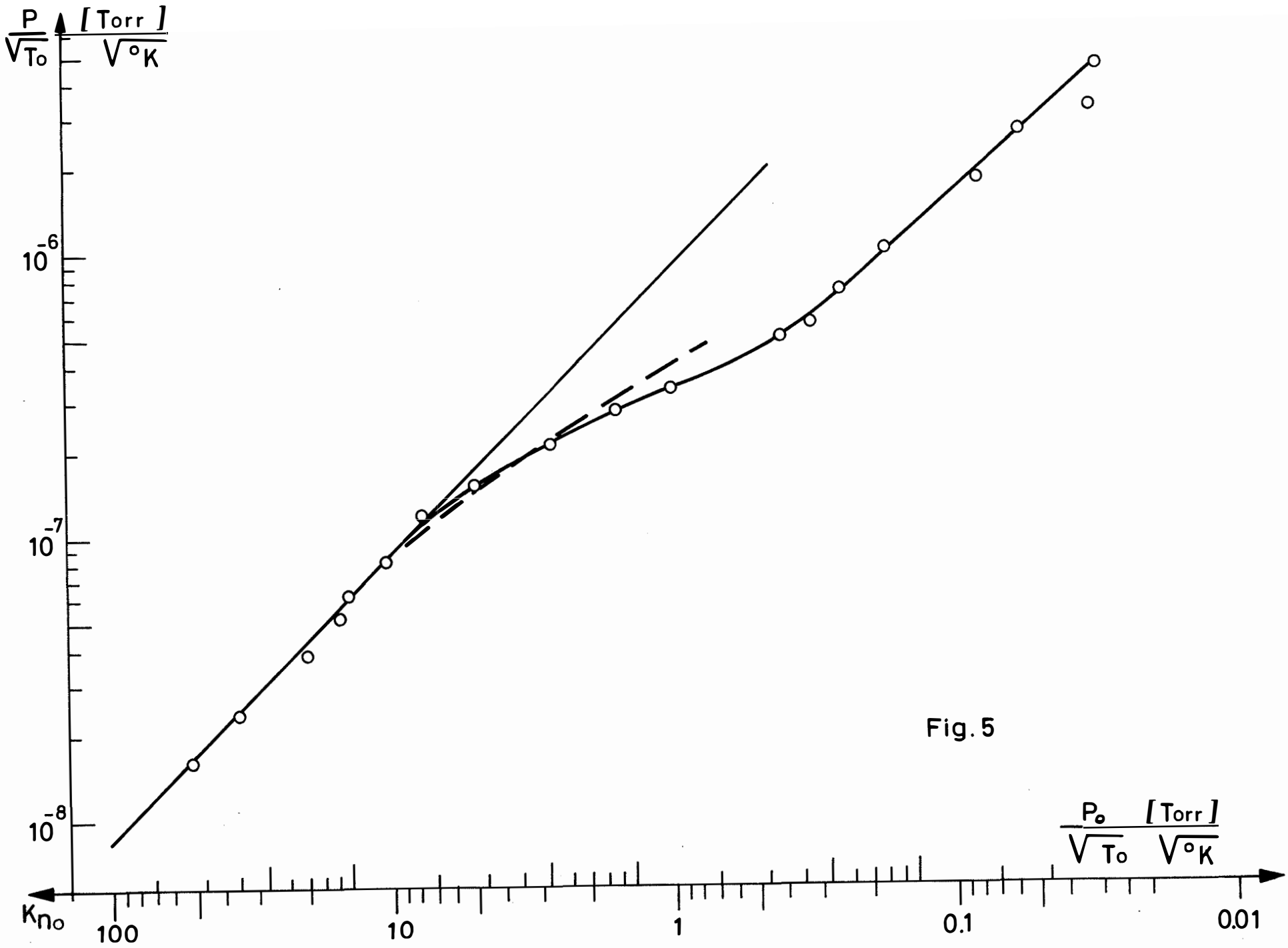

Fig. 5